Wind field estimation through autonomous quadcopter avionics

Conference Paper · September 2016

DOI: 10.1109/DASC.2016.7778071

6 authors, including:

Xingyu Xiang
West Virginia University
16 PUBLICATIONS **76** CITATIONS
SEE PROFILE

Zhonghai Wang
Intelligent Fusion Technology
65 PUBLICATIONS **444** CITATIONS
SEE PROFILE

Zijian Mo
University at Buffalo, The State University of New York
11 PUBLICATIONS **63** CITATIONS
SEE PROFILE

Genshe Chen
Intelligent Fusion Technology, Inc.
327 PUBLICATIONS **3,116** CITATIONS
SEE PROFILE

Wind Field Estimation Through Autonomous Quadcopter Avionics

Xingyu Xiang, Zhonghai Wang, Zijian Mo, Genshe Chen
Intelligent Fusion Technology, Inc.
Germantown, MD 20876
{xingyu.xiang, zwang, zijian.mo, gchen}@intfusiontech.com

Erik Blasch
Air Force Research Lab
Rome, NY 13441
erik.blasch.1@us.af.mil

Khanh Pham
Air Force Research Lab
Kirtland AFB, NM 87117
khanh.pham.1@us.af.mil

***Abstract*—Using integrated sensors carried onboard a quadrotor unmanned aerial vehicle (UAV) can be used to wind field estimation through intelligent dynamic analysis, UAV control, and sensor management. The data from UAV on-board sensors such as GPS and inertial measurement units are utilized such that no dedicated sensors (i.e., pitot tube) for wind characterization are necessary. Using the estimated ground weather conditions, the UAV performance provides a means for rapid wind field estimation. The motivation is to develop an agile and low-cost atmospheric measurements system for energy harvest and real-time mission support. The advantage of UAV versus weather balloons is the agility of the UAV to operate in constrained environments and complex terrain. The wind profile is calculated by applying algorithms that relates the attitude of the aircraft to the local wind speed and direction, sparing the payloads of external devices like multi-hole tubes. Several existing wind field estimation algorithms are evaluated and compared with the proposed Kalman Filter dynamic behavior fusion using data obtained from the wind sensors as well. Error analysis and the reasons of errors are discussed in the estimation process. The proposed UAV-based on-board avionics system can be used to improve positioning accuracy and flight stability in the spatially varying, turbulent wind circumstances.**

I. Introduction

A new era of unmanned aerial vehicles (UAV) is on the horizon and both fixed wing and rotary wing UAVs continue to increase in prevalence and are becoming more and more capable. The trend is driven by the advances in related technologies [1], [2], [3] and its own advantages, including but not limited to, low construction and operation cost, ability to enter dangerous environments, hardware and software flexibility for customized mission [4]. The autonomous vehicle technology has matured to the point where certain civil, commercial and military applications are feasible and compelling. Greater accessibility to UAV platforms led to innovative usages spanning telecommunications, remote sensing and monitoring, lifesaving, and natural resources management. The UAVs holds the potential to benefit the society in many ways [5].

As a subcategory of UAV, the quadcopter or quadrotor is propelled by four rotors which are placed in a square formation with equal distance from the mass center. Comparing with the fixed wing drones, it has less flying range and endurance while holds the superiority of manoeuvrability, which makes it ideal for operations in environments with tight space or varied type of obstacles. Another reason of selecting quadrotor in our work lies in its susceptibility to wind fields and gusts, and the wind field estimation results could also be utilized to compensate the impact of wind disturbances.

The wind field information is normally assumed to be known in autonomous energy harvesting research [6], the understanding of wind characteristics for UAV guidance and navigation is stated in [7]. Many projects and researches have been deployed to understand this renewable resource and related phenomena. The UAVs has been considered as an alternative to the conventional platforms for atmospheric wind profiling by using Lidar and Sodar technologies [8], [9]. The Small Unmanned Meteorological Observer which is based on Styrofoam airplane measures horizontal wind speed and direction based on ground speed differences [10]. The Meteorological Mini Unmanned Vehicle developed in Germany measures the wind vector with the mounted probe together with internal sensor data [11]. The Vario XLC is the small-sized helicopter uses the sonic anemometer to estimate the wind field [12].

Most of the aforementioned platforms use the fixed wing UAV whose flying patterns need to be carefully designed. This paper tries to use quadrotor itself as a measurement device for the wind field estimation. No dedicated meteorological sensors is used during the estimation process. Previous research work of STARMAC identified the possibility of the isolation of wind disturbances from other forces acting on the vehicle [13]. The wind estimation are derived from the vehicle status that is affected by forces acting on the vehicle.

The contributions of this work include a derivation of the wind speed and direction based on the quadrotor dynamics models previously developed in [14]. The wind field estimation algorithm relies exclusively on onboard data and hardware specifications. The quadrotor dynamic behavior and its control system is modeled, different approaches for the wind estimation is discussed and developed. The field testing results are presented by comparing with the measured data from digital anemometer under the same circumstances.

This paper proceeds as follows. Section II presents the preliminary information about the modeling of vehicle dynamics. In Section III, wind estimation and wind field calculation are presented. The selected UAV model and the outdoor testing plans, together with the comparison results are presented in penultimate section. The conclusion along with the desirable future work are discussed in Section V.

978-1-5090-2523-7/16/$31.00 ©2016 IEEE

II. Mathematical Model of Quadcopter

The structure of a quadcopter is presented in Fig. 1. The motors and propellers are mounted to spin in specific directions and the quadcopter is controlled by adjusting the angular velocities of the rotors. The model shown in Fig. 1 is also the one used in our work with the model name MATRICE 100 developed by DJI company. Motors are labeled sequentially in a counterclockwise direction starting from the front left motor. There are two clockwise spinning motors and two counterclockwise spinning motors due to the effects of rotational torque. When a quadrotor need to rotate in the yaw axis, two diagonal motors with the same spin direction increase the angular velocity and the other two decrease the spin speed such that the overall thrust could be maintained and an evenly applied torque is created in one direction.

The absolute linear position of the quadcopter is defined in the inertial frame x, y, z axes as shown in in Fig. 1, the inertial frame is an Earth-fixed set of axes that is used as an unmoving reference. (x, y, z) is noted based on the *ENU* coordinates convention, where x axis points geodetic East, y axis points geodetic North and z axis points Up. The attitude, i.e., the angular position, is defined in the inertial frame with three Euler angles. The rotation around x axis is the roll angle ϕ, pitch angle θ determines the rotation around y axis and yaw angle ψ around the z axis.

The body frame of reference (x_B, y_B, z_B) is the coordinate system that is aligned with the vehicle body and the origin is rigidly fixed to its center of gravity. The x_B axis typically points out the nose, the y_B axis points out the right side of the fuselage, and the z_B axis points out the bottom of the fuselage. Both reference systems are shown in Fig. 1.

The absolute position of the vehicle is defined in the inertial frame of reference with the vector $\mathbf{\Omega}$ and the corresponding attitude is defined by $\mathbf{\Lambda}$.

$$\mathbf{\Omega} = \begin{bmatrix} x \\ y \\ z \end{bmatrix} \qquad \mathbf{\Lambda} = \begin{bmatrix} \phi \\ \theta \\ \psi \end{bmatrix} \tag{1}$$

And the notation Ω_B, Λ_B are used for the position and attitude information of the body frame reference. The linear velocity vector $\dot{\Omega}_B$ and the angular velocity vector $\dot{\Lambda}_B$ are defined as:

$$\dot{\mathbf{\Omega}}_B = \begin{bmatrix} \dot{x}_B \\ \dot{y}_B \\ \dot{z}_B \end{bmatrix} \qquad \dot{\mathbf{\Lambda}}_B = \begin{bmatrix} \dot{\phi}_B \\ \dot{\theta}_B \\ \dot{\psi}_B \end{bmatrix} \tag{2}$$

To transform matrix from the body frame to the inertial frame, the rotation matrix $\mathbf{R}$ is derived by following the right-hand rule:

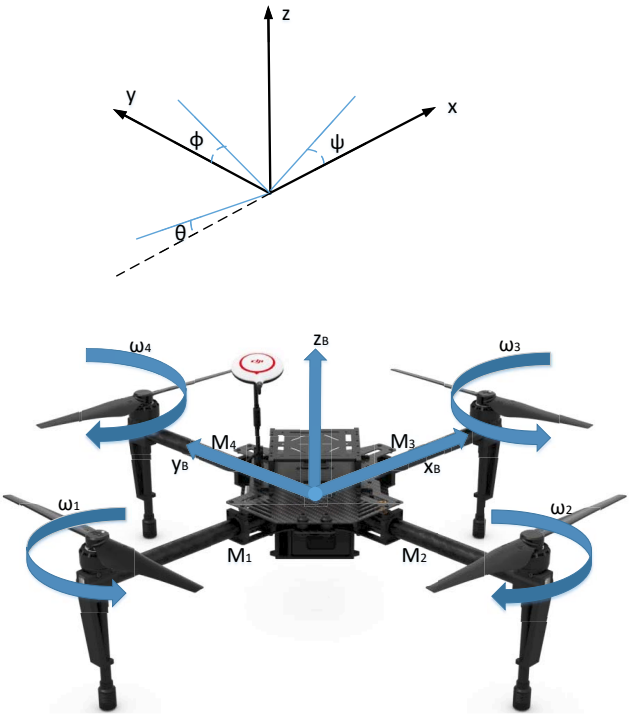

Fig. 1. Inertial and Body frames of the quadrotor

$$\mathbf{R} = \begin{pmatrix} \cos\psi\cos\theta & \cos\psi\sin\theta\sin\phi - \sin\psi\cos\phi & \cos\phi\sin\theta\cos\psi + \sin\phi\sin\psi \\ \sin\psi\cos\theta & \sin\phi\sin\theta\sin\psi + \cos\phi\cos\psi & \sin\psi\sin\theta\cos\phi - \cos\psi\sin\phi \\ -\sin\theta & \cos\theta\sin\phi & \cos\theta\cos\phi \end{pmatrix} \tag{3}$$

Additionally, the rotation matrix $\mathbf{W}$ is defined as the angular velocities transformation from the inertial frame to the body frame:

$$\mathbf{W} = \begin{pmatrix} 1 & 0 & -\sin\theta \\ 0 & \cos\phi & \cos\theta\sin\phi \\ 0 & -\sin\phi & \cos\theta\cos\phi \end{pmatrix} \tag{4}$$

The inverse of $\mathbf{W}$ performs the opposite transformation, i.e., from the body frame to the inertial frame.

The quadrotor used in the following field testing has symmetric structure with four arms aligned with the XY plane, thus the inertia matrix is diagonal and $I_{xx} = I_{yy}$. The thrust $\mathbf{T}$ created by the combined rotor forces lies in the direction of the body z axis. The torques τ_ϕ, τ_θ, τ_ψ correspond the related body frame angles.

$$\mathbf{T} = \sum_{i=1}^{4} f_i = k\sum_{i=1}^{4} w_i^2, \quad \mathbf{T}_B = \begin{pmatrix} 0 \\ 0 \\ T \end{pmatrix} \tag{5}$$

$$\begin{pmatrix} \tau_\phi \\ \tau_\theta \\ \tau_\psi \end{pmatrix} = \begin{pmatrix} lk(-w_2^2 + w_4^2) \\ lk(-w_1^2 + w_3^2) \\ \sum_{i=1}^{4} \tau_{M_i} \end{pmatrix} \tag{6}$$

where l is the distance between the rotor and the mass center of the vehicle. The angular velocity of rotor i is denoted by w_i, the torque τ_{M_i} around the rotor axis is derived by multiplying the drag constant b with the angular velocity, i.e., $\tau_{M_i} = bw_i^2$. Based on equation 6, the roll movement is acquired by decreasing the velocity of the second rotor and increasing the fourth rotor's velocity, the pitch movement is acquired by decreasing the first rotor's velocity while increasing the velocity of the third rotor, and the yaw movement is acquired by increasing the angular velocities of two opposite rotors and decreasing the velocities of the other two.

In the body frame, the force required for the aircraft acceleration $m\dot{\mathbf{\Omega}}_B$ and the centrifugal force $\dot{\mathbf{\Lambda}}_B(m\Omega_B)$ is equal to the gravity $\mathbf{R^T G}$ and the total rotor thrust $\mathbf{T}$. While in the inertial frame, the centrifugal force is omitted and the acceleration of the quadcopter is caused by the gravity and thrust force.

$$\begin{aligned} m\ddot{\mathbf{\Omega}} &= \mathbf{G} + \mathbf{R}\mathbf{T_B}\begin{pmatrix}\ddot{x}\\ \ddot{y}\\ \ddot{z}\end{pmatrix} = -\mathbf{g}\begin{pmatrix}0\\0\\1\end{pmatrix} \\ &+ \frac{T}{m}\begin{pmatrix}\cos\phi\sin\theta\cos\psi + \sin\phi\sin\psi\\ \sin\psi\sin\theta\cos\phi - \cos\psi\sin\phi\\ \cos\theta\cos\phi\end{pmatrix} \end{aligned} \tag{7}$$

When drag force generated by the air resistance is included to derive the realistical behaviour of the quadrotor, the diagonal coefficient matrix related the linear velocities to the force is included in equation 7:

$$\begin{aligned} m\ddot{\mathbf{\Omega}} &= \mathbf{G} + \mathbf{R}\mathbf{T_B}\begin{pmatrix}\ddot{x}\\ \ddot{y}\\ \ddot{z}\end{pmatrix} = -\mathbf{g}\begin{pmatrix}0\\0\\1\end{pmatrix} \\ &+ \frac{T}{m}\begin{pmatrix}\cos\phi\sin\theta\cos\psi + \sin\phi\sin\psi\\ \sin\psi\sin\theta\cos\phi - \cos\psi\sin\phi\\ \cos\theta\cos\phi\end{pmatrix} \\ &- \frac{1}{m}\begin{pmatrix}C_x & 0 & 0\\ 0 & C_y & 0\\ 0 & 0 & C_z\end{pmatrix}\begin{pmatrix}\dot{x}\\ \dot{y}\\ \dot{z}\end{pmatrix} \end{aligned} \tag{8}$$

where C_x, C_y, C_z are the drag force coefficients for velocities in the corresponding directions of the inertial frame.

III. Wind Field Estimation

Based on the conservation of energy for a fluid in motion [15], the wind speed could be estimated by:

$$v = \sqrt{\frac{2D}{\rho A(\gamma) C_D(\gamma)}} \tag{9}$$

where v is the wind speed with the unit meters per second (m/s), D denotes the drag force acting on the quadcopter in Newton (N), ρ is the air density (kg/m^3) of the quadcopter's position, $A(\gamma)$ is the area exposed to the wind in (m^2) as a function of the quadcopter tilt angle γ and $C_D(\gamma)$ is the drag coefficient. The angle γ is noted in Fig. 2, which relates to roll angle (ϕ) and pitch angle (θ) by following equation:

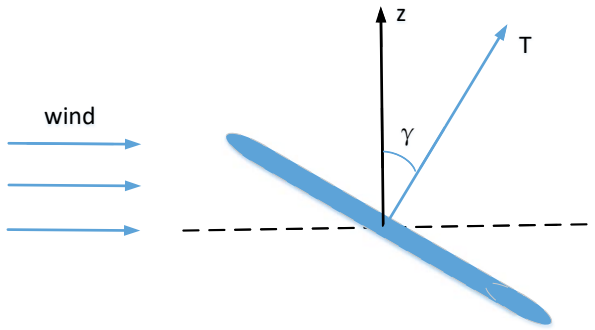

Fig. 2. Quadcopter tilts due to the drag force caused by the wind

$$\gamma = \cos^{-1}\left(\frac{\vec{u}_{xy}\cdot(\vec{e}_\phi \times \vec{u}_\theta)}{|\vec{u}_{xy}|\cdot|\vec{e}_\phi \times \vec{e}_\theta|}\right) \tag{10}$$

where

$$\vec{e}_\phi = \begin{pmatrix}0\\ \cos\phi\\ \sin\phi\end{pmatrix}, \qquad \vec{e}_\theta = \begin{pmatrix}\cos\theta\\ 0\\ -\sin\theta\end{pmatrix}$$

and $\vec{u}_{xy}$ is the unit vector normal to the plane of xy axis, i.e., $\vec{u}_{xy} = \begin{pmatrix}0\\0\\1\end{pmatrix}$. The wind direction could be calculated through the following steps:

- Derive the angle λ that is between the direction of the quadrotor and the projection of the vector $(\vec{e}_\phi \times \vec{e}_\theta)$ on the xy plane

$$\lambda = \psi - \text{atan}\left(\frac{(\vec{e}_\phi \times \vec{e}_\theta)_y}{(\vec{e}_\phi \times \vec{e}_\theta)_x}\right), \tag{11}$$

  where ψ is the yaw angle and $(\vec{e}_\phi \times \vec{e}_\theta)_x$, $(\vec{e}_\phi \times \vec{e}_\theta)_y$ are the projection of the cross product on the x and y axis, respectively.
- Determine the relative position of the projection of $\vec{e}_\phi \times \vec{e}_\theta$ on the xy plane corresponding to the position of the quadrotor:

$$\vec{u}_{xz}\cdot(\vec{e}_\phi \times \vec{e}_\theta)_{xy} = \begin{cases} <0 & \text{if } \vec{e}_\phi \times \vec{e}_\theta \text{ is left side} \\ >0 & \text{if } \vec{e}_\phi \times \vec{e}_\theta \text{ is right side} \\ 0 & \text{otherwise} \end{cases} \tag{12}$$

- Then the direction D_{wind} could be calculated:

$$\text{D}_{\text{wind}} = \begin{cases} 360^\circ - \lambda + \phi & \text{if } \vec{u}_{xz}\cdot(\vec{e}_\phi \times \vec{e}_\theta)_{xy} > 0 \\ \lambda + \phi & \text{if } \vec{u}_{xz} > 0 \end{cases} \tag{13}$$

Once the drag force has been derived, the wind speed could be calculated according to equation 9. The basic case is to assume that the quadrotor is hovering in a steady position and the velocity and attitude remain unchanged and then the drag force is:

$$D = mg\tan(\gamma) \tag{14}$$

where γ could be calculated with equations 10.

The drag force could also be calculated by dynamic linear equations by considering the dynamic effects:

$$D_x = (\cos\psi \sin\theta \cos\phi + \sin\psi \sin\phi)T - \ddot{x}m \quad (15)$$
$$D_y = (\sin\psi \sin\theta \cos\phi - \cos\psi \sin\phi)T - \ddot{y}m \quad (16)$$
$$D_z = (\cos\theta \cos\phi)T - \ddot{z}m - gm \quad (17)$$

The total thrust T could be calculated by using the third linear equation while disregarding the drag force D_z:

$$T = \frac{(\ddot{z} + g)m}{\cos\theta \cos\phi} \quad (18)$$

Accelerations in the inertial frame of reference are obtained from the aircraft onboard sensor data and the value in the body frame reference could be derived by transformation. Then The drag force used for the wind field calculation could be derived from D_x and D_y:

$$D = \sqrt{{D_x}^2 + {D_y}^2} \quad (19)$$

Another method to estimate the drag force makes use of the Kalman filter to estimate the system state including the drag forces mentioned above [16], [17]. The system state defines the varying quantities of the system, for example, the linear and angular position, vehicle velocity. The measurements or observations are the available information provided by the vehicle onboard sensors. The Kalman filter model assumes that the state of the system at a time k evolved from the prior state at time $k-1$ according to the equation:

$$\mathbf{x_k} = \mathbf{F_k x_{k-1}} + \mathbf{B_k u_k} + \mathbf{w_k} \quad (20)$$

where $\mathbf{x_k}$ is the state vector containing the terms of interest, $\mathbf{u_k}$ is the vector containing the control inputs, $\mathbf{F_k}$ is the state transition matrix that applies the effect of the system state parameter at time $k-1$ on the system state at time k. $\mathbf{B_k}$ is the control input matrix which applies the effect of the control input parameter in the vector $\mathbf{u_k}$ on the state vector, $\mathbf{w_k}$ is the vector containing the process noise that is assumed to be drawn from a zero mean multivariate normal distribution with covariance given by the covariance matrix. Measurements of the system can also be performed according to the model:

$$\mathbf{z_k} = \mathbf{H_k x_k} + \mathbf{v_k} \quad (21)$$

where $\mathbf{z_k}$ is the vector of measurements, $\mathbf{H_k}$ is the transformation matrix that maps the state vector parameters into the measurement domain, $\mathbf{v_k}$ is the measurement noise terms that is assumed to be zero mean Gaussian white noise. Normally the Kalman filter algorithm could be divided in two main steps:

- Prediction, the filter uses the state estimated from the previous time stamp to produce the estimation of the state at the current time stamp. Since this predicted step does not include observation information from the current time step it is also called the "a priori state estimate".
- Update, the filter averages the predication results with current observation information to refine the state estimation. The Kalman filter gain is used to achieve the weighted average, the value of which is calculated from the noise covariance matrix.

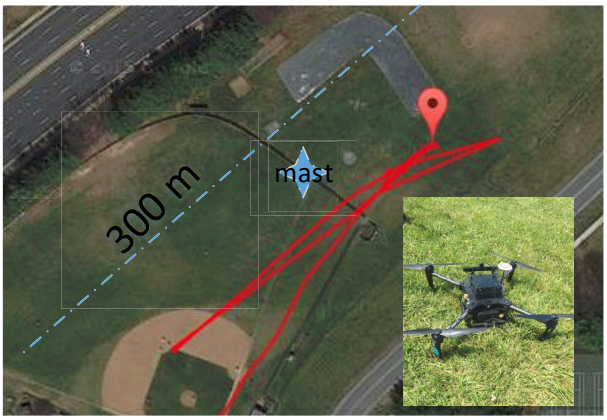

Fig. 3. The environment of the field testing, red mark is the place the quadcopter took off, the red trace is the flying path, the star mark is the position of the measurement tower

IV. Field Measurements

The quadcopter chosen for the testing is the model MATRICE 100 developed by DJI company, the model of which is shown in Fig. 1. The reasons of selection is due to its hardware and software expandabilities. The additional expansion bays provides enough room for extra components, payloads and customized devices to fly with. Through the DJI Guidance SDK, the system could be fully customized and the onboard data could be achieved through the provided software and the Guidance SDK. Besides, the enhanced GPS could provide more accurate positioning and the integrated sensor modules enable the capability of detecting and avoiding obstacles. All these features ensure the accurate and safe flight missions.

To validate the algorithms with the real data, several flight missions have been carried out. The location of the field tests is the open area closed to the athletic fields of Montgomery College of Germantown in Maryland, USA. The field is shown in Fig. 3 and the space is enough for the current fly mission, the quadrotor connection, especially the propeller and battery settings, need to be checked for safety purpose [19]. The basic vehicle status could be visualized on real time through the DJI mobile application when connecting to the remote controller. The detail flying data is stored onboard and could be processed later after the mission.

The digital anemometer is used as the reference to validate the algorithms's calculation results, HoldPeak Digital HP-866B is a portable yet accurate device with resolution 0.1 m/s. It is said that the accuracy of the measured wind speed is ± 0.1, and another anemometer with the model Proster Digital TL090 is also used as the complementary reference. The preliminary outdoor experiments indicates that those two anemometers display relative consistent results with ± 0.5 value difference. The anemometers are attached to the mast in the testing field, since the anemometers cannot store the measured data, a video camera GoPro is attached to the equipment for the purpose of

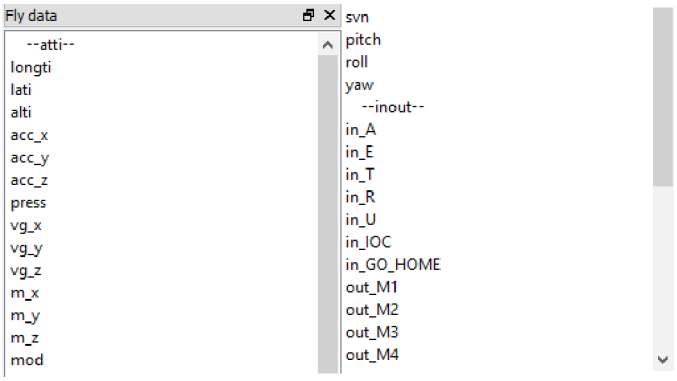

(a) Flight data accessed through the onboard memory device

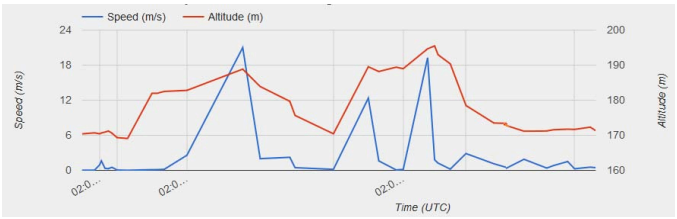

(b) Altitude and Velocity during the flight testing

Fig. 4. Data information of the flight mission and one example plotting

recording data for later analysis. The anemometer are tried to put under the same condition as the flying mission of the quadcopter. The mast with the attached anemometer and GoPro camera is in the middle of the flying trajectory (shown in Fig. 3 as the blue star mark), the flying altitude is also tried to be identical to the height of the anemometer.

Two different measurement plans have been planned. One is to make aircraft fly straight and compare the derived results with the external measurement devices at the same height. The expectation is to provide wind speed and direction value that is in good agreement with the data reported by the wind measurement device. For the aim of achieving accurate calculation results, the designed flying trajectory is set to be a straight line, which means there is no turning during the testing and the flying direction is kept constant for at least 10 seconds. The other plan is to determine the wind field information while the aircraft is hovering, the vehicle is stayed in the same spot for at least 10 seconds and the data from the onboard sensors are used to calculate the wind information based on the basic methodology mentioned in Section III. Fig. 4(a) shows the user friendly software interface provided by DJI company to access the data after the mission, the position and the attitude information, the inout information of the aircraft including the motors' angular velocities are all accessible by the software interface. An plot of the altitude and velocity with respect to the time is shown in Fig. 4(b).

The field test is carried on June 10, 2016 at the open area near Montgomery College, each flight time is around 60 seconds to guarantee enough valid data is collected, the flying trajectory is shown as the red paths in Fig. 3. The average wind direction measured by the anemometers is $241°$

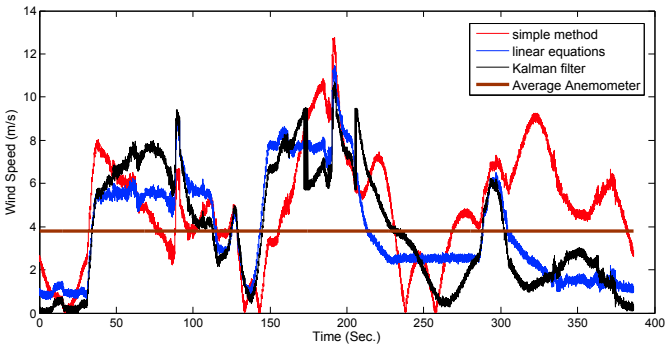

Fig. 5. Wind speed estimation results

and the calculated value is $251°$. The difference exists while the calculated direction indicates the validity of the direction calculation algorithm.

The wind speed estimation results are shown in Fig. 5, curves with different color correspond different calculation approaches. The average wind speed calculated by digital anemometer is around $3.981\ \mathrm{m/s}$, the maximum wind speed is $8.377\ \mathrm{m/s}$. The wind estimation approaches indicate relative validity, the method without considering the dynamics shows the largest deviation when comparing the measured reference results, which is predictable due to the basic model type and the calculation process. However, it works well while the quadrotor is hovering, the calculated results close to the reference value by ± 0.6. The Kalman filter approach provides the closest value but the processing causes certain delay once the data set becomes large.

V. Conclusion

The presented work demonstrates the feasibility of a quadcopter as a measurement for the wind field estimation without any dedicated wind sensors on board. Different approaches are evaluated through the outdoor field testings. Two measurement scenarios are designed for complementary evaluation, one is to measure the wind characteristic during the straight line fly mission, the other scenario is to calculate the wind when the quadroter is hovering. The results validate the relations between the aircraft's attitude and wind profile, and the comparison between the measured value and the calculated value indicates the agreement and consistency. The estimation results are more accurate when the quadrotor is hovering. However, the whole system model needs refinements to provide quality results, the ignorance of the possible noise and the aforementioned system assumptions limits the calculation accuracy. The incorporating of recent research work, more measurement missions designed under different weather conditions could be utilized to further improve and evaluate the validity of the proposed algorithms.

References

[1] M. C. Valenti and X. Xiang, "Constellation shaping for bit-interleaved ldpc coded apsk," *IEEE Transactions on Communications*, vol. 60, no. 10, pp. 2960–2970, October 2012.

[2] L. Li, Y. Ding, J. K. Zhang, and R. Zhang, "Blind detection with unique identification in two-way relay channel," *IEEE Transactions on Wireless Communications*, vol. 11, no. 7, pp. 2640–2648, July 2012.
[3] X. Xiang and M. C. Valenti, "Closing the gap to the capacity of apsk: Constellation shaping and degree distributions," in *Computing, Networking and Communications (ICNC), 2013 International Conference on*, San Diego, CA, Jan 2013, pp. 691–695.
[4] L. Li, G. Wang, G. Chen, H. M. Chen, E. Blasch, and K. Pham, "Robust airborne image transmission using joint source-channel coding with uep," in *2016 IEEE Aerospace Conference*, Big Sky, MT, March 2016, pp. 1–7.
[5] J. Yang, L. Paarmann, H. M. Kwon, and W. Xiong, "Biological-vision inspired dsa system for uavs," in *2009 International Conference on Bio-inspired Systems and Signal Processing (Biosignal 2009)*, Porto, Portugal, Jan 2009.
[6] P. Lisssaman, D. V. Ventures, and C. Patel, "Neutral energy cycles for a vehicle in sinusoidal and turbulent vertical gusts," in *45th AIAA Aerospace Sciences Meeting and Exhibit*, Reno, Nevada, Jan. 2007.
[7] J. W. Langelaan, "Long distance/duration trajectory optimization for small uavs," in *AIAA Guidance, Navigation and Control Conference and Exhibit*, Hilton Head, South Carolina, August 2007.
[8] G. Kocer, M. Mansour, N. Chokani, R. Abhari, and M. Müller, "Full-scale wind turbine near-wake measurements using an instrumented uninhabited aerial vehicle," *Journal of Solar Energy Engineering*, vol. 133, no. 4, 2011.
[9] X. Xiang, Z. Mo, Z. Wang, G. Chen, K. Pham, and E. Blasch, "An improved mimo-sar simulator strategy with ray tracing," in *SPIE Defense+ Security*, vol. 98380B, Baltimore, MD, May 2016.
[10] S. Mayer, A. Sandvik, M. O. Jonassen, and J. Reuder, "Atmospheric profiling with the uas sumo: a new perspective for the evaluation of fine-scale atmospheric models," *Meteorology and Atmospheric Physics*, vol. 116, no. 1-2, pp. 15–26, 2012.
[11] A. Van den Kroonenberg, T. Martin, M. Buschmann, J. Bange, and P. Vörsmann, "Measuring the wind vector using the autonomous mini aerial vehicle m2av," *Journal of Atmospheric and Oceanic Technology*, vol. 25, no. 11, pp. 1969–1982, 2008.
[12] M. K. Samal, M. Garratt, H. Pota, and H. T. Sangani, "Model predictive attitude control of vario unmanned helicopter," in *37th Annual Conference on IEEE Industrial Electronics Society*, Melbourne, VIC, 2011, pp. 622–627.
[13] G. Hoffmann, D. G. Rajnarayan, S. L. Waslander, D. Dostal, J. S. Jang, and C. J. Tomlin, "The stanford testbed of autonomous rotorcraft for multi agent control (starmac)," in *Digital Avionics Systems Conference, 2004*, vol. 2, 2004.
[14] H. Huang, G. M. Hoffmann, S. L. Waslander, and C. J. Tomlin, "Aerodynamics and control of autonomous quadrotor helicopters in aggressive maneuvering," in *Robotics and Automation, IEEE International Conference on*. IEEE, 2009, pp. 3277–3282.
[15] F. M. White, "Fluid mechanics,(2003)," 2003.
[16] R. C. Leishman, J. C. Macdonald, R. W. Beard, and T. W. McLain, "Quadrotors and accelerometers: State estimation with an improved dynamic model," *Control Systems, IEEE*, vol. 34, no. 1, pp. 28–41, 2014.
[17] J. Moyano Cano, "Quadrotor uav for wind profile characterization," 2013.
[18] L. Meier, P. Tanskanen, F. Fraundorfer, and M. Pollefeys, "Pixhawk: A system for autonomous flight using onboard computer vision," in *Robotics and automation (ICRA), 2011 IEEE international conference on*, 2011, pp. 2992–2997.
[19] S. Wei, D. Shen, L. Ge, W. Yu, E. Blasch, K. Pham, and G. Chen, "Secured network sensor-based defense system," in *SPIE Defense + Security*, Baltimore, MD, May 2015.